Structural integrity assessment of turbine discs in presence of potential defects: probabilistic analysis and implementation

S. BERETTA[1], S. FOLETTI[1], M. MADIA[2] and E. CAVALLERI[3]

[1]*Dipartimento di Meccanica, Politecnico di Milano, Milano, Italy,* [2]*Division 9.1, Federal Institute for Materials Research and Testing (BAM), Berlin, Germany,* [3]*Ansaldo Sviluppo Energia, Genova, Italy*

Received Date: 16 October 2014; Accepted Date: 18 May 2015; Published Online: 20 June 2015

NOMENCLATURE

a	= crack size
a_f	= final crack
a_{perm}	= permissible defect
a_0	= initial defect
$A_{0,1,2,3}$	= coefficients of the polynomial for local stress
C	= constant of the Paris' law
CV	= coefficient of variation σ/μ
E	= elastic modulus
ERS	= equivalent reflector size
$f(L_r)$	= plastic correction function
F	= boundary correction factor
FAD	= failure assessment diagram
$K_{\mathcal{J}}$	= plastic-corrected stress intensity factor
K	= stress intensity factor for mode I
K_{Ip}, K_{Is}	= contribution to K due to primary, secondary loads
K_{IC}	= fracture toughness
$K_{\max}$	= maximum stress intensity factor
$\mathcal{J}$	= $\mathcal{J}$-integral
LCF	= low-cycle fatigue
L_r	= ligament yielding parameter
$L_{r,\text{biax}}$	= ligament yielding parameter in case of biaxial loading
m	= exponent of the Paris'law
$M_{0,1,2,3}$	= coefficients of the Shiratori's weight function

Correspondence: S. Beretta. E-mail: stefano.beretta@polimi.it

n_{nodes} = number of nodes
n_{steps} = number of load steps
n_{life} = target life of the turbine disc
N_{res} = residual lifetime for a given defect size
NDT = non-destructive tests
P = load
P_Y = limit load
P_f = failure probability
r_p = closure-corrected cyclic plastic zone
r.v. = random variable
R = strength
R_s = stress ratio
S = applied stress
S_{av} = averaged stress for calculation of local yielding parameter
S_m = mechanical stress due to centrifugal loads
S_{max} = maximum applied stress at overspeed
$S_{p,\,max}$ = maximum principal stress in-plane
S_{res} = residual stress
S_{therm} = thermal stress
S_x = stress parallel to crack plane
S_y = stress perpendicular to crack plane
S_F = flow strength
S_Y = yield strength
S_U = ultimate tensile strength
S_θ = hoop stress
t = section thickness
T = temperature
δ = distance of subsurface node from contour
ε_f = fracture strain
ε_{max} = maximum strain
η = safety factor
λ = biaxiality factor
μ = mean value
σ = standard deviation
ω_0 = nominal operational speed
ω_{max} = maximum speed
ΔK = stress intensity factor range
ΔJ_{eff} = effective J-integral range
ΔN = increment of stress cycles
ΔS = applied stress range
ΔS_{eff} = effective applied stress range
Φ = elliptic integral of the second kind
$\sqrt{area}$ = Murakami's crack size parameter: projected area of the defect size on a plane perpendicular to stress direction

SUFFIXES

k = index for cycle increments
i = index for nodes
j = index for load steps
p = index for assessment points

INTRODUCTION

Rotor discs for turbines are heavy components usually designed on LCF[1,2] adopting design curves with suitable probabilistic margins.[3,4] However, rotor discs cannot be manufactured without defects (inclusions and forging defects[5]), and it is therefore important to assess the criticality of defects considering that they will grow under

fatigue at each startup–shutdown cycle of the turbine. On the other hand, the failure mode that mostly contributes to the number of losses is represented by accidental overspeeds[6,7] or the unstable crack growth from disc centre regions (also at rotational regimes lower than the burst speed).[5,8]

From the design point of view, such risk can be assessed according to the schematic in Fig. 1: (i) a potential defect (or an NDT indication) can be present at any point of the turbine disc (see an axisymmetric analysis in Fig. 1a); (ii) any structural detail is subjected to stress cycles (due to turbine startups) in which the primary stress S is governed by the centrifugal loads; (iii) a prospective defect at any point can propagate under N_{life} startup–shutdown cycles; (iv) failure could occur at the next stress cycle if, at some critical defect location, the fracture toughness is exceeded. In this scenario, the turbine rotor should be able to withstand, in terms of unstable fracture, the stress transient at startup or the eventual maximum stress S_{max} caused by overspeed. In particular, startup cycles can be very challenging for static fracture because the low temperature (and low toughness) is accompanied by the peak transient stresses[2] that can cause the cracking of disc centre regions.[8] The possible overspeed for a gas turbine has typically a ratio $\omega_{max}/\omega_o \leq 120\,\%$, while the complete yielding of the disc would occur at bursting speeds larger than 145 %.[5]

Janssen and Joyce[9] mentioned the adoption of *usual* safety factors (namely, a safety factor of 1.5 for yield strain and fracture toughness) for determining acceptability of defects in different disc regions, but because design primary stresses are quite high ($S = 0.7 - 0.8 S_Y$), it would be hardly possible to accomplish such a simple assessment if a design engineer considered the many different sources of variability (sizing error of NDT inspections, dispersion of material properties and uncertainty in stress conditions). Moreover, the resulting failure probability would be unknown, and in the case of generous safety factors, it could be excessively smaller than target reliabilities.

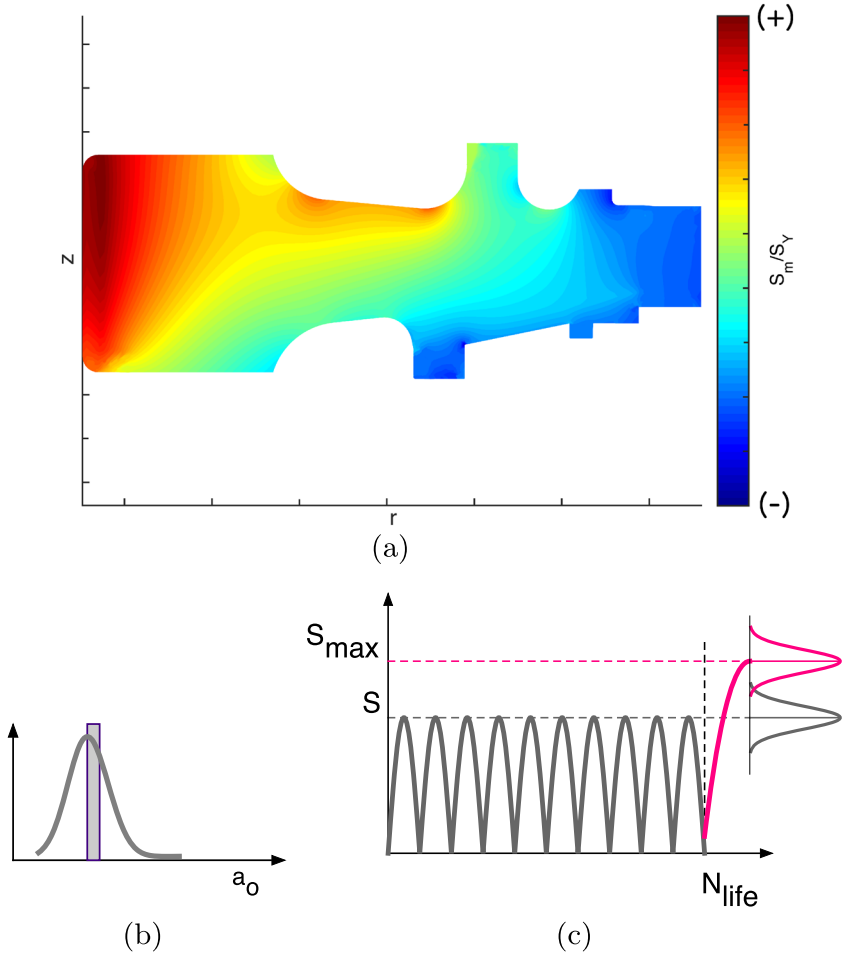

Fig. 1 Problem statement for the assessment of a turbine disc: (a) state of stress due to primary centrifugal loads; (b) potential defect (NDT indication), which can be present at any point of the FE mesh; (c) schematic of the prospective stress cycles during the life with uncertainties in the stress conditions.

Scope – probabilistic analysis

Actually, in order to avoid any unnecessary design conservatism, it is worth adopting a probabilistic approach[10] for describing the whole disc life under the different sources of scatter and for obtaining failure probabilities in the order of 10^{-5} (as prescribed by standards[11,12] for a *safety critical* primary component). The aim of the probabilistic analysis is then to correctly account for the typical variability of some parameters (sizing error of NDT inspections and dispersion of material properties)[10] and to check the design robustness against the typical uncertainties of engineering assumptions (based on experimental tests and FE analyses[13]) for stress conditions.

Considering the standards for integrity assessment,[12,14] they propose simplified *semi-probabilistic* separate approaches for the assessment of static fracture and fatigue in which suitable percentiles of the parameters have to be considered, the assessment being made with suitable *safety factors*. However, in the problem described in Fig. 1, the primary stress S is not independent from the stress at overspeed because at any point (under elastic stress conditions):

$$S_{\max} = \left(\frac{\omega_{\max}}{\omega_o}\right)^2 \cdot S \tag{1}$$

Consequently, separate assessments for fatigue and fracture would lead to excessive conservatism and a probabilistic approach considering the entire mission (startup–shutdown cycles + prospective overspeed) is needed. A number of general purpose probabilistic structural integrity software[15,16] could handle the analysis, but they are not designed for an automatic assessment by the input of a FE analysis; therefore, it would be impossible to run a full probabilistic analysis for all the nodes of a detailed FE analysis of a turbine disc.

On the other hand, this is the specific feature of codes like *DARWIN*[13,17,18] or *P-FAT*,[19] which allow to carry out a probabilistic fatigue assessment. In particular, the code *DARWIN* allows for the automatic calculation of fatigue crack growth for aircraft engine rotors, it includes also a module for the probabilistic life calculation on the basis of random variables, performed using Monte Carlo simulations. The software encloses some interesting features, which allow us to simplify the geometry of the component that could be extremely complex in case of turbine discs. However, these codes are not specifically designed for assessment under a mission profile like the one in Fig. 1c considering the risk of static fracture at the occurrence of an overspeed.

The software Assessment for Structural Integrity of Discs (AStrID) has been developed with the goal of a reliable tool for the automatic assessment of rotor discs. It handles the geometries and the results of finite element thermal and stress linear analyses carried out with commercial FE codes on axisymmetric models of the discs. In particular, the analysis is carried out under the assumption that at each point there is a stress cycle due to the startup–shutdown cycles: the reliability is evaluated as the capability to withstand (with a very load failure probability) a prospective accidental overspeed at the end of service life.

This paper describes the development of the computation procedure by summarizing the structural integrity concepts for the assessment of turbine discs (Section on Structural Integrity of Rotor Discs). Then a fully probabilistic approach is developed for analysing the effect of the different random variables (stress components and material properties) on the failure probability of a turbine disc (Section on Probabilistic Fracture Assessment of a Turbine Disc). From this background, the features of the AStrID implementation and the semi-probabilistic approach are then discussed, together with some results (Section on Assessment for Structural Integrity of Discs Assessment Software).

STRUCTURAL INTEGRITY OF ROTOR DISCS

Fatigue life and crack propagation

Fatigue design of disc turbine discs (both for air and land based turbines) is usually based on LCF[1,2] and design curves with suitable probabilistic margins.[3] When a crack has to be considered in LCF, the most suitable approaches are those based on $\Delta\mathcal{J}_{\text{eff}}$ concept,[20–22] which derive the *crack driving force* from the cyclic stress–strain response of the material and an estimation of ΔS_{eff},[23] and the growth rate $da/dN = f(\Delta\mathcal{J}_{\text{eff}})$ is derived from the *effective crack growth curve* from long crack data. Within these approaches, Harkegard *et al.*[24] proposed a simple conservative model based on the crack growth curve at $R_s = 0$.

However, it has to be considered that the stress state at typical structural features of rotor discs undergoes elastic shakedown. Therefore, the typical crack growth models under LCF based on $\Delta\mathcal{J}$ can be reduced to a ΔK approach obtaining good life predictions even considering a few thousand load cycles[25] (this is a further support to the simple assumptions in Ref. [24]). With this background, the crack growth in the different points of the turbine discs has been simulated considering, at any point of a FE mesh, a plasticity corrected ΔK:[26]

$$\Delta K_{\text{corr}} = F \cdot \Delta S \cdot \sqrt{\pi \cdot (a + r_p/4)} \tag{2}$$

where F is the boundary correction factor for a semi-elliptical (surface) or elliptical (internal) crack (Section on Stress Intensity Factors and Crack Shape) and r_p is a

closure corrected cyclic plastic zone. The crack growth rate in the different points of the turbine (which experience different temperatures) was calculated from long crack data ($R_s = 0$) as follows:

$$\frac{da}{dN} = C(T)\cdot(\Delta K_{\text{corr}})^m \tag{3}$$

where the parameter $C(T)$ accounts for the dependence on temperature[24] and the *enhanced* crack growth for short cracks[27] at High temperature (HT) for typical rotor disc steels.

Static fracture

A simple assessment against fracture for turbine discs was adopted by Forsberg[28] in terms of

$$\varepsilon_{\max} \le \varepsilon_f \tag{4}$$

However, this simple approach is based on continuum mechanics and does not allow to consider the potential presence of defects, which may be found by non-destructive testing before or during the operational life of the machine. Instead, a typical fracture mechanics approach has been used in this study, which is based on the structural integrity assessment of components containing defects. Some papers already discussed the assessment of turbines under static fracture with Linear Elastic Fracture Mechanics (LEFM),[5,9], but because design primary stresses are quite high ($S = 0.7 - 0.8S_Y$), the assessment against the final fracture should be carried out considering *crack driving force* at $S_{\max}$ under elastic–plastic conditions.[29]

Common flaw assessment methods (R6,[30] SINTAP/FITNET,[29] API 579–1[14] and BS 7910[12]) require an accurate determination of the crack driving force (in terms of K or $\mathcal{J}$, depending on the amount of crack-tip plasticity) and material fracture toughness (K_{IC}) for analysis at initiation in ductile materials or fracture of brittle materials, complete *R-curve* for analysis of ductile materials in which a certain amount of stable crack growth is permitted). The crack driving force can be calculated according to different levels of analysis, involving simple analytical formulations (typically available in compendia for simple geometries) up to large and expensive finite element analysis (assessment of components with complex geometries and load cases). In particular, the authors showed already that the typical stress intensity factors (SIF) analytical solutions for semi-circular and semi-elliptical surface cracks in a plate in tension (Newman–Raju[31] and Shiratori *et al.*[32]) can be employed for discs subjected to rotational body forces.[33] The elastic–plastic fracture assessment has been carried out here according to an R6 approach:

$$K_{\mathcal{J}} = \frac{K_{\max}}{f(L_r)} \le K_{IC} \tag{5}$$

where $K_{\mathcal{J}}$ is a plastic-corrected stress intensity factor and $f(L_r)$ is the plastic correction function. The ligament yielding parameter L_r, according to R6,[30] is defined as follows:

$$L_r = \frac{P}{P_Y} = \frac{S}{S_Y} \tag{6}$$

which represents the ratio between the applied load and the limit load of the structure for a given crack configuration, in terms of global or local limit load[29] (see Refs [34,35] for improved definitions of reference yield load or stress). Beside the general definition of L_r in Eq. (6), more appropriate formulations have been implemented in order to adapt the fracture assessment to the discs. The first step has been to set the limit condition to the flow stress $S_F = 0.5\cdot(S_U + S_Y)$. Furthermore, as the disc undergoes different temperatures in each point (and during each step of the startup cycle), the limit stress has been considered dependent on the temperature, thus leading to the following relationship:

$$L_r = \frac{S_{av}}{S_F(T)} \tag{7}$$

where S_{av} is suitable averaged local stress.

Dealing with components subjected to rotational body forces, the most important issue is that a disc is subjected to a multiaxial loading condition. In particular, the principal stress components are the hoop stress (S_θ) and the maximum principal stress on the plane perpendicular to the tangential direction ($S_{p,\max}$). Because of the aforementioned statements, the state of stress in the disc can be regarded as biaxial loading. Note that because Eq. (6) is valid only in case of monotonic loading, then proper solutions for L_r in biaxial problems must be adopted in this case. Among the solutions available in the literature, the one proposed by Miura and Takahashi[36] for semi-elliptical cracks in plates under biaxial loading has been judged to be the most effective to be implemented in the analytical calculations. The expression of L_r writes

$$L_{r,\text{biax}} = \frac{S_y}{S_F}\cdot\sqrt{\lambda^2 - \lambda + 1} \tag{8}$$

where $\lambda = S_x/S_y$ is the biaxiality factor, S_y is the stress normal to the crack plane and S_x is the stress acting parallel to the crack plane. As potential cracks can be detected in each point of the disc considering different planes, the proper values for S_x and S_y can be defined as follows:

1 if the crack plane is orthogonal to the tangential direction $S_y = S_\theta$ and $\lambda = S_{p,\max}/S_\theta$;
2 if the crack plane is orthogonal to the in-plane principal direction $S_y = S_{p,\max}$ and $\lambda = S_\theta/S_{p,\max}$.

Note that the applied-stress formulation reported in Eq. (8) represents the equivalent von Mises stress in case of plane stress conditions (for more details, the reader may refer to Ref. [35]). The plastic correction function $f(L_r)$ is then implemented as $f(L_{r,\text{biax}})$ in the procedure;

furthermore, among the three possible options within the European procedure SINTAP/FITNET, option 1B (the stress–strain curve of the material is not characterized by a yield plateau) has been chosen because of the great advantage that the function depends only on the static mechanical properties of the material (E, S_Y and S_U, which depend on the temperature of the load step, see Section on Calculations of Residual Life and Defect Acceptability).

A good example is provided in Fig. 2, where the $\mathcal{J}$-integral calculated with option 1B has been compared with the values provided by option 3 and elastic–plastic finite element calculations. Despite the simplicity and the lower level of detail of the reference stress approach used in this study, the accuracy is very satisfactory compared with those other approaches, which need a higher effort.[37]

For the disc fracture assessment, $K_{\max}$ has been evaluated considering the separate contribution of primary (centrifugal inertial loads) and secondary (thermal stresses due to radial temperature gradient) as follows:

$$K_{\max} = K_{I,p} + V\left(\frac{K_{I,s}}{K_{I,p}}, L_r\right)\cdot K_{I,s} \tag{9}$$

where V is a weighting parameter ($V \to 1$ for $L_r \to 0$), $K_{I,p}$ and $K_{I,s}$, respectively, are SIFs due to primary and secondary stresses.

PROBABILISTIC FRACTURE ASSESSMENT OF A TURBINE DISC

Scheme and random variables

From a probabilistic point of view, the reliability in a given location of the rotor disc can be calculated in the following steps (Fig. 3):

1 the distribution of the initial defect size a_0 corresponds to the *sizing error* of an NDT indication (or a prospective population of defects) able to propagate because of the mission cycles;
2 at the end of the N_{life} missions, there is a prospective distribution of cracks a_f, whose realizations can be calculated (both numerically or in closed form) with an equation:

$$a_f = \int_0^{N_{\text{life}}} C(T)\cdot\Delta K_{\text{corr}}^m dN \tag{10}$$

where ΔK_{corr} is expressed by Eq. (1), and $C(T)$ and m are the Paris' constants (note that C depends on temperature); and
3 the prospective occurrence of the load $S_{\max}$ (the maximum load of the load spectrum or an accidental overspeed) will lead to a prospective distribution of the stress intensity factors, which contribute to $K_{\max}$ (Eq. (9)) as follows:

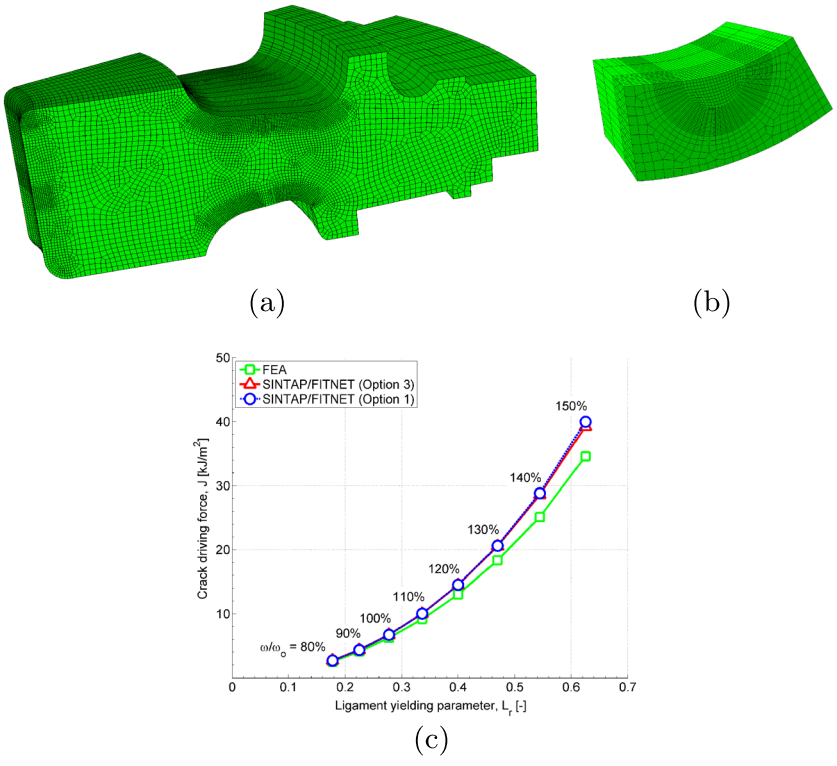

Fig. 2 FE elastic–plastic analyses for the verification of $\mathcal{J}$: (a) global model; (b) submodel for a semi-circular crack at the neck (a = 10 mm); (c) comparison between FE results and estimations according to options 1B and 3 of the SINTAP/FITNET procedure.

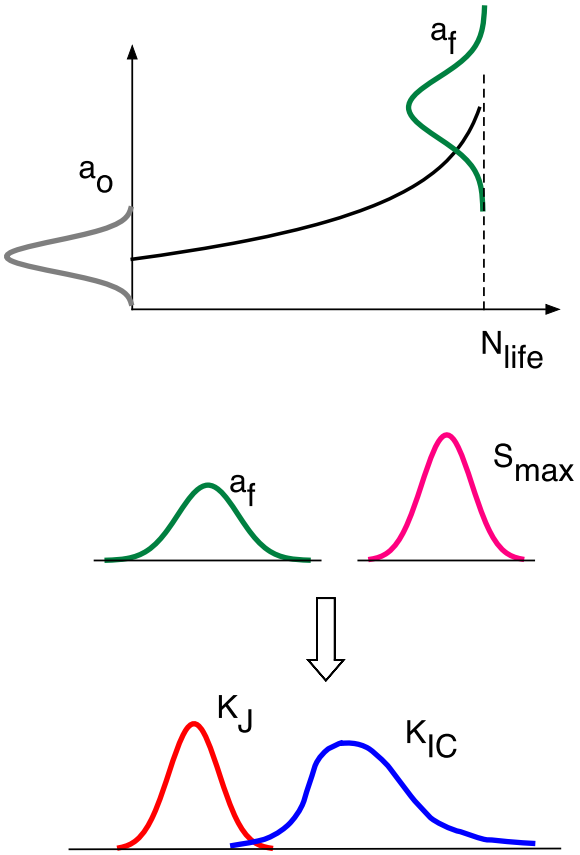

Fig. 3 Schematic of the probabilistic assessment: (a) a population of initial defects a_o leads to a prospective distribution a_f after N_{life} cycles at stress level S; (b) the combinations of distributions a_f and S_{max} lead to a K_J distribution (including elasto-plastic driving force); and (c) the failure probability can be then calculated according to Eq. (12).

$$\begin{cases} K_{I,p} = F \cdot S_{\max} \cdot \sqrt{\pi a_f} \\ K_{I,s} = F \cdot (S_{\text{therm}} + S_{\text{res}}) \cdot \sqrt{\pi a_f} \end{cases} \tag{11}$$

where S_{max} is the maximum mechanical primary stress due to centrifugal loads, S_{therm} and S_{res}, respectively, are thermal and residual secondary stresses;

4 the *failure probability* can be calculated from the overlapping between the distribution of K_J and the distribution of the fracture toughness K_{IC} (K_{mat}) in terms of the probability that

$$P_f = Pr\left\{K_J = \frac{K_{\max}}{f(L_r)} \geq K_{IC}\right\} \tag{12}$$

or, alternatively

$$P_f = Pr\left\{\frac{K_{\max}}{K_{IC}} \geq f(L_r)\right\} \tag{13}$$

if the problem is solved employing the (FAD) approach.[12,29]

The previous assessment steps involve different random variables (they will be highlighted in **bold**) that can be described as follows:

- the initial defect distribution $\mathbf{a_0}$ corresponds to the sizing error of the NDT, which has a relatively large scatter,[12] and it could be described by a lognormal or truncated Gaussian distribution;
- the stresses $\mathbf{S_{max}}$ (or $\mathbf{S_m}$) and $\mathbf{S_{therm}}$ at a turbine point are evaluated by FE elastic analyses, and they are affected by a *design uncertainty*,[17] which can be described by a normal distribution, whose coefficient of variation has to be at least 0.1[12];
- quenching and specific manufacturing processes can induce significant residual stresses at the disc hub: the scatter of $\mathbf{S_{res}}$ has been evaluated as quite significant [measurements carried out at Ansaldo Energia Spa (AEN)], and it has been modelled as a truncated normal distribution with $CV = 0.3$;
- the two r.v.'s $\mathbf{S_m}$ and $\mathbf{S_{max}}$ (mechanical stress during startup cycles and maximum stress at overspeed) are perfectly correlated because of Eq. (1);
- the applied stress for propagation is a combination of three r.v.'s:

$$\Delta\mathbf{S} = \mathbf{S_m} + \mathbf{S_{therm}} + \mathbf{S_{res}}; \tag{14}$$

- because the two parameters $\log(C), m$ of the growth curves are strongly correlated,[38] the variability of growth rate can be simply be described by taking $\mathbf{C}$ as lognormally distributed (which corresponds to $\log_{10}C$ as normally distributed) with a scatter in accordance with Ref [39], while m is kept constant; and
- the $\mathbf{K_{IC}}$ variable can be taken with a $CV = 0.1$ at high temperature (taking the usual assumptions for *upper shelf*), while the distribution in the transition region (which is relevant for estimating the critical crack size at cold startups[2]) is described by a Weibull with $\beta = 4$[40].

A summary of the random variables assumed in the probabilistic analysis is reported in Table 1. As for defect shape, NDT indications are measured in terms of *ERS*,[41] referring to calibration with flat-bottom circular holes. In terms of fracture calculations, the initial aspect ratio of the crack has been assumed to be $a/c = 0.4$ as a conservative assumption[2] (for an embedded elliptical crack under

Table 1 Summary of the random variables for probabilistic analysis

Variable	Distribution	Dispersion	Reference
$\mathbf{S_{max}}$	Normal	$CV = 0.1$	[12,17]
$\mathbf{S_{therm}}$	Normal	$CV = 0.1$	[12]
$\mathbf{S_{res}}$	Trunc. normal	$CV = 0.3$	[10,12]
$\mathbf{a_o}$	Trunc. normal	$CV = 0.2$	[10,12]
$\mathbf{C}$	Lognormal	$\sigma_{\log_{10}C} = 0.0768$	[39]
$\mathbf{K_{IC}}$	Normal (upper shelf) Weibull (ductile–brittle trans.)	$CV = 0.1$	[10] [40]

tension $F = 1$, while $F = 0.636$ for a penny-shaped crack[42]). The effect of this assumption on the reliability assessment will be discussed in the next section.

Probabilistic analysis

A series of Monte Carlo simulations have been carried out for different critical positions (hub and neck) in order to have reference solutions for the determination of *partial safety factors*. Simulations were carried out adopting an important sampling approach and 10^6 random combinations of the six r.v.'s in Table 1.

It is interesting to see the Monte Carlo simulation for the prospective propagation of a defect with a given size a_0 at the rotor disc hub of a gas turbo machine, under base load condition, with a prospective accidental overspeed in a FAD (see Fig. 4: the figure has been obtained by a crude Monte Carlo with 10^5 simulations for clarity). Calculations were carried out, after extracting the stress state at the hub edge from the FE analysis, by adopting the F factor described in Section on Stress Intensity Factors and Crack Shape. The steps of the simulation can be so summarized:

- the uncertainties of the variables $\Delta\mathbf{S}$, $\mathbf{a}_0$ cause a significant scatter of the initial condition simulated by the grey points;
- after $N_{life} = 3000$ load cycles, the SIF increases in the vertical direction due to propagation and the scatter of $\mathbf{C}$; and
- the application of the overspeed makes a few points to exceed the $f(L_r)$ curve, which corresponds to a failure probability P_f of the order of 10^{-5}.

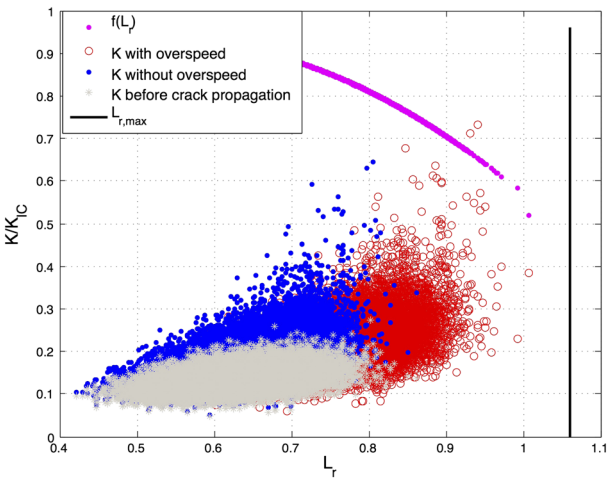

Fig. 4 Monte Carlo simulation for the assessment of the hub of a turbine disc: propagation under base load for N_{life} cycles and then overspeed represented on a failure assessment diagram. The failures correspond to the few points exceeding the $f(L_r)$ curve.

It is clear from this pictorial view of the probabilistic simulation that the static fracture at the prospective overspeed looks the key point in the assessment of the turbine disc.

Sensitivity

Monte Carlo simulations have been run for determining the sensitivity of P_f to the different statistical variables. In particular, P_f has been calculated by varying the mean value of each single r.v. as $\mu + \sigma$ and $\mu - \sigma$ while keeping the other variables at their mean value. The results, normalized with respect to the simulation of Fig. 4, are shown in Table 2, where it can be seen that the r.v. that mostly affects the failure probability are $\mathbf{a}_0 - \mathbf{logC} - \mathbf{S}_{max}$. These *main variables* have been highlighted in grey. Also $\mathbf{K_{IC}}$ can be considered a main variable because it strongly depends on the temperature, and its scatter can be very high in the ductile–brittle transition (which is critical at startups[2,5]).

The strong dependence of P_f on $\mathbf{K_{IC}}$ is due to the fact that the *failure* events in the Monte Carlo simulations are controlled by the *static fracture*. This is further confirmed by a series of analyses carried out at different N_{life} (Fig. 5), where it is clear that neglection of the elastic–plastic contribution to the driving force at overspeed would lead to a severe underestimation of the failure probability (the static fracture assessment and the inclusion of K_J are the terms that mark the difference between the present procedure and the one of *DARWIN*'s suite). Meanwhile, it can be also easily observed that the failure probability is controlled by N_{life}: from this point of view, the present analysis is a fundamental tool for the *life extension* of turbine discs.

About the dependence of failure probability on the crack shape, a series of calculations were carried out considering (i) a semi-elliptical crack with $a = 0.42$ (mm) and $a/c = 0.4$; (ii) a semi-circular crack with $a = 0.42$ (mm); (iii) a semi-circular crack with $a = 0.67$ (mm) (same defect area as the semi-elliptical defect). The results are shown in Fig. 6, where it can be seen that the crack depth is not the relevant size parameter but rather the defect area.

Table 2 Sensitivity of P_f to variation of the different random variables (P_f normalized respect the failure probability $P_{f,ref}$ calculated for the simulation in Fig. 4)

		$P_f/P_{f,ref}$	
$\mathbf{a}_0$	10^{-2}	1	10^2
logC	10^{-1}	1	6
$\mathbf{K_{IC}}$	2	1	0.6
$\mathbf{S_{max}}$	$2 \cdot 10^{-2}$	1	18
$\mathbf{S_{res}}$	2	1	0.5
$\mathbf{S_{therm}}$	0.5	1	2
	$\mu - \sigma$	μ	$\mu + \sigma$

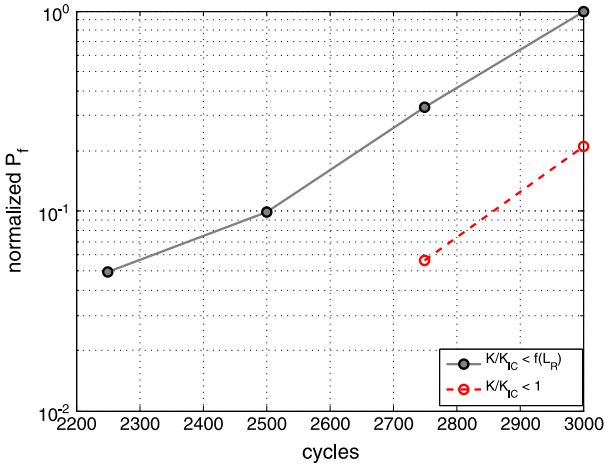

Fig. 5 Dependence of P_f on the variable N_{life} (P_f normalized respect to the simulation of Fig. 4).

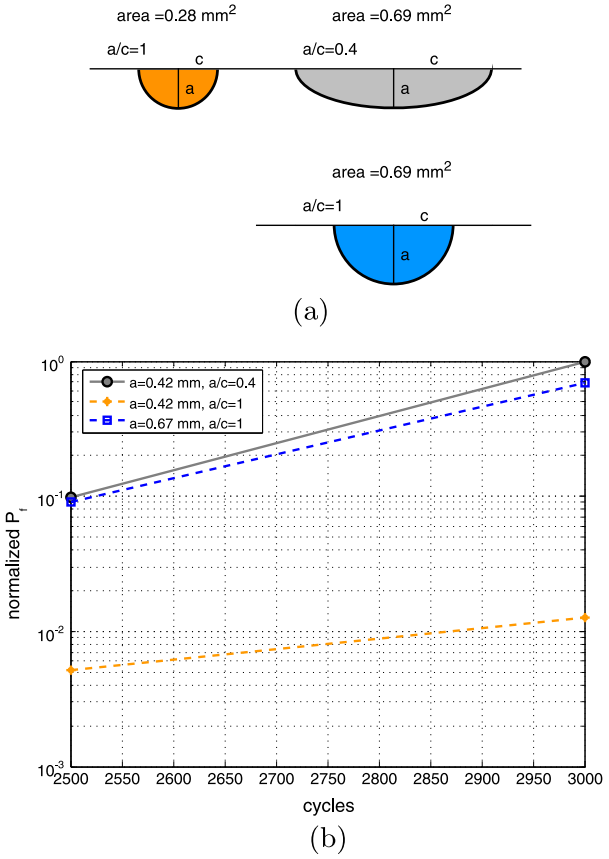

Fig. 6 Effect of shape on failure probability for a surface crack at the hub: (a) defect shapes considered and (b) dependence of P_f on the different assumptions (P_f normalized respect to the simulation of Fig. 4).

This result is also consistent with (i) the concept of $\sqrt{area}$ by Murakami,[43,44] who showed that cracks of different shapes have the same maximum SIF if their size, expressed in terms of $\sqrt{area}$, is equivalent; (ii) the defect area is the relevant parameter also for ultrasonic NDT measurements[41,45]). Therefore, defect size, within the AStrID software, has been expressed in terms of *ERS* (diameter of the circle with the same area as the ellipse of the defect).

SOFTWARE FOR STRUCTURAL INTEGRITY ASSESSMENT OF DISCS

The assessment procedure for turbine disc has been implemented into AStrID. The software, written in Matlab, processes the results from 2D axisymmetric thermoelastic analyses of a rotor disc whose transient startup has been discretized in different load steps. The software receives as an input (i) the nodal coordinates; (ii) stresses averaged at nodes for each load step; and (iii) nodal temperatures for each load step. The aim is to obtain life and defect acceptance maps that can support the designer and the NDT inspectors: local features (holes and notches) can be investigated with dedicated 3D analyses, to be post-processed in a similar way as the entire disc. In the following, the different phases of the calculations are discussed.

Pre-processing

The first phase of the analysis is the input nodal coordinates $N_i(r_i, z_i)$ for each i-th node together with nodal values $(T_i, S_i, S_{therm,i}, S_{res,i})_j$ for each of the j load steps in which the loading cycle has been divided ($i = 1, 2 \ldots n_{nodes}$; $j = 1, 2 \ldots n_{steps}$). Subsequently, there is a pre-processing phase with (Fig. 7)

- identification for each surface node of the corresponding subsurface nodes in the direction normal to contour and calculation of the section thickness t_i; and
- identification for each internal node of the minimum distance to contour δ_i and calculation of the section thickness t_i.

These geometric parameters will then be used to calculate the SIF for surface and subsurface nodes as follows.

Stress intensity factors and crack shape

Each node of the FE corresponds to a potential defect location, and therefore, in order to obtain maps of allowable life or permissible defect, a crack propagation is simulated in each node of the mesh, assuming an initial aspect ratio $a/c = 0.4$. The calculations, which are based on the maximum principal stress (in-plane or

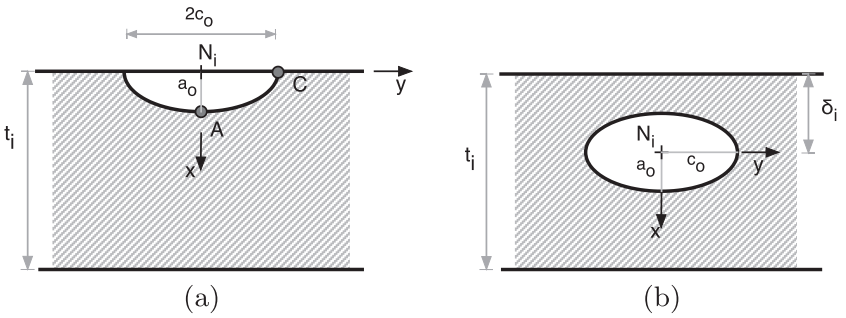

Fig. 7 Geometry of the defect for stress intensity factors calculation: (a) surface node and (b) subsurface node.

circumferential) according to the crack potential propagation direction, are different for surface and internal nodes.

Surface nodes

In the case of surface nodes, it can be easily verified, adopting the Newman–Raju[31] formulas, that the crack shape evolution from a semi-elliptical crack depends only on the ratio a/a_o, and it tends to a shape factor $(a/c)_\infty$ that depends on the stress gradient. It is therefore simple to express

$$a/c = f(a/a_o) \tag{15}$$

where

$$\lim_{a/a_o \to \infty} a/c = (a/c)_\infty$$

for simplicity, it has been assumed that $(a/c)_\infty = 0.88$, which is valid for uniform stress. Among the huge variety of solutions, which can be found in the literature, the analytical model employed in the case of surface cracks is the one developed by Shiratori for a plate with a semi-elliptical surface crack subjected to a polynomial stress profile (after identifying subsurface nodes with step1 of pre-processing):

$$S(\xi) = \left(A_3 \cdot \xi^3 + A_2 \cdot \xi^2 + A_1 \cdot \xi + A_0\right) \tag{16}$$

where $\xi = 1 - x/a$. The coefficient of the stress profile is used in the definition of the stress intensity factor in pure mode I according to the following equation:[32]

$$K = (A_3 \cdot M_3 + A_2 \cdot M_2 + A_1 \cdot M_1 + A_0 \cdot M_0)\frac{1}{\Phi} \cdot F_{\text{prox}} \cdot \sqrt{\pi \cdot a} \tag{17}$$

where Φ is the elliptic integral of the second kind and M coefficients are tabled values depending on crack size and shape. F_{prox} is a proximity factor to free surface with a functional form:

$$F_{\text{prox}} = f\left(\frac{a}{t_i}\right) \tag{18}$$

It is then very fast to integrate Eq. (10) by taking (15), because it allows us to make a 1D integration (instead of integrating separately for tips A and C).

Subsurface (internal) nodes

In the case of subsurface nodes, the crack propagation is calculated assuming a semi-elliptical crack parallel to the disc edge. The crack propagation is then calculated assuming that the aspect ratio remains constant up to breakout[46] with a geometric factor at point A_1:

$$F_{A_1} = f\left(\frac{a}{\delta_i}\right) \tag{19}$$

derived from Isida–Noguchi solution[47] for an embedded elliptical crack under uniform stress. After breakout, the crack has then a depth (from the prospective position of point A_2):[46]

$$a_{\text{break}} = 2 \cdot \delta_i \tag{20}$$

Crack propagation is then calculated as a surface node, after recalculation of the initial shape factor (Fig. 8b), with the SIF formulation described in the previous subsection.

Semi-probabilistic approach

In order to make a probabilistic crack propagation analysis for each node, it would be impossible (in terms of

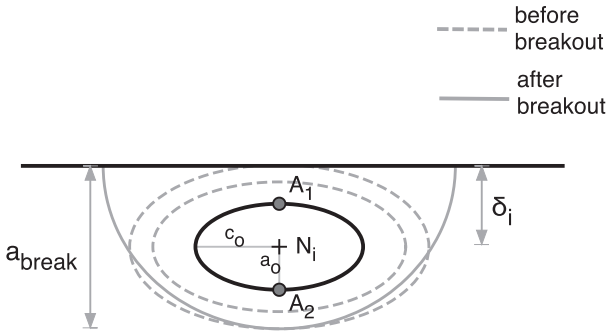

Fig. 8 Subsurface node with prospective crack shape evolution.[46]

computational time) to run a Monte Carlo simulation as the one shown in Section on Probabilistic Fracture Assessment of a Turbine Disc. It was then decided to run the probabilistic analysis adopting the method of *partial safety factors*. This semi-probabilistic method is the usual approach proposed by EUROCODE[11] (and all the standards), and it is based on the simple idea of finding the *design point* for an $\mathbf{S}-\mathbf{R}$ (where the stress $\mathbf{S}$ and the resistance $\mathbf{R}$ are described by suitable statistical distributions) as follows:

$$S_{\text{char}} \cdot \eta_S \leq \frac{R_{\text{char}}}{\eta_R} \tag{21}$$

where

- S_{char} and R_{char} are *characteristic values* (i.e. the percentiles to be considered) for the two distributions;
- η_S and η_R are suitable *partial safety factors* (η_S and η_R are greater than 1).

Equation (21) is a substitute of a full probabilistic assessment based on:

$$P_f = Pr[\mathbf{S} > \mathbf{R}] \leq P_{f,\text{target}} \tag{22}$$

Details for the derivation the partial safety factors can be found in Ref [48]. The same approach is adopted by BS 7910[12] for a simple static fracture assessment considering the different variables involved (i.e. primary stress, toughness and crack size): for each of these variables, the *characteristic values* are prescribed together with an appropriate *partial safety factor*.

It was decided to follow the same approach also for the present assessment. The concept is simply shown in Fig. 9 on a FAD:

- we can simply calculate the propagation of the average defect $a_{o,\text{mean}}$ under a number of cycles N_{life} considering the mean values for (S, C);
- then, the application of mean $S_{\max}$ identifies the central value for the multivariate $K_{\max}/K_{IC} - L_r$ population; and
- a suitable combination of the variables allows to identify points in the tails of the multivariate $K_{\max}/K_{IC} - L_r$ population.

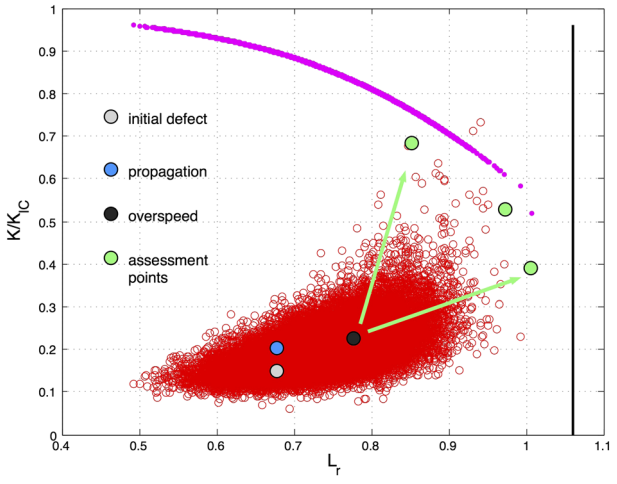

Fig. 9 Strategy for defining the *assessment points*.

This procedure is carried out for three suitable combinations of characteristic values for the main variables $(a_0, S_{\max}, C, K_{IC})$ (the variables highlighted in grey in Table 2) with an assessment of the type:

$$\left.\frac{K_{\max}}{f(L_R)}\right|_p \leq \frac{K_{IC,\text{char}}}{\eta_{K_{IC}}} \tag{23}$$

where the index $p = 1, 2, 3$ refers to the assessment points (Fig. 9) and $\eta_{K_{IC}}$ is a partial safety factor for toughness. In this approach, the two variables $S_{\text{res}} - S_{\text{therm}}$ are kept at the mean value because they play a minor role in the static fracture assessment. The characteristic values have been determined, by trials and errors, verifying the application of Eq. (23) in several combinations (a_0, N_{life}) (for different regions of several turbine discs) for which the Monte Carlo simulations had been shown:

$$P_f = Pr\left[\mathbf{K_J} > \mathbf{K_{IC}}\right] \leq 5 \cdot 10^{-5} \tag{24}$$

Calculations of residual life and defect acceptability

The first result of the analysis with AStrID is a map of the residual life for a given initial defect a_0, which is the number of cycles needed for a_0 to propagate up to a crack size, which ensures a target failure probability (at the occurrence of an overspeed at the end of service life) $P_f = 5 \cdot 10^{-5}$. The crack propagation is carried out for by repeatedly calculating in each node:

$$a_k(k \cdot \Delta N) = a_{k-1} + C \cdot \Delta K_{k-1} \cdot \Delta N \tag{25}$$

where ΔN is a suitable cycle increment. The residual life, for any node, is calculated with Eq. (23) as follows:

$$N_{\text{res},i} = \max_k (k \cdot \Delta N) : \left\{ \left.\frac{K_{\max}(k \cdot \Delta N)}{f(L_R)}\right|_{p=1\ldots3} \leq \frac{K_{IC,\text{char}}}{\eta_{K_{IC}}} \right\} \tag{26}$$

The map of N_{res} for a given defect size is shown in Fig. 10a for a turbine disc of a gas turbo machine under base load conditions (ΔS is evaluated with Eq. (14) considering steady state distribution of thermal stresses).

In terms of acceptability of defects, it is then important to obtain the map of the maximum permissible defect a_p given a target residual life N_{life}, which is the maximum defect able to propagate for N_{life} so that the

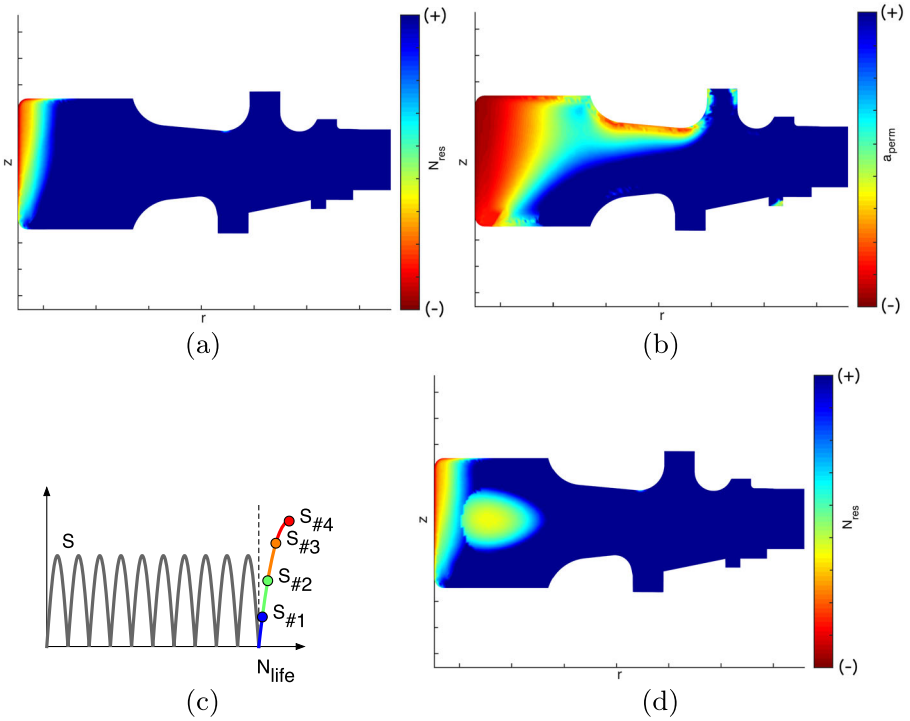

Fig. 10 Results from Assessment for Structural Integrity of Disks: (a) map of N_{life} for a given defect size; (b) map of permissible defect for a given N_{life} under base load; (c) discretization of the $N_{life}+1$-th load into steps for describing transient stresses–temperatures at startup; and (d) map of permissible defect for a given N_{life} with startup cycles.

failure probability remains below the target failure probability if the overspeed occurs at the $N_{life}+1$ cycle under a given load condition. The permissible defect

$$a_{perm,i} : N_{res,i} = N_{life} \tag{27}$$

is iteratively calculated by the bisection method between the two limits $a_{perm,lower} = 0.2(mm)$ and $a_{perm,upper} = 20(mm)$ adopting Eq. (26). The map is shown in Fig. 10b: it is easy to appreciate from the colours that the most critical regions are the hub and the two transitions at the disc neck.

However, a realistic defect acceptability analysis should be carried out considering the transient stress and temperatures during startups, because thermal stresses are very high during the initial phases of the transient and, at the same time, toughness reaches its minimum value.[2] To do this, the loading cycle is divided into load steps, and the residual life is evaluated at each node through considering the prospective stress distribution for the different load steps (Fig. 10c). So the life then becomes

$$N_{res,i} = \max_{k}(k\cdot\Delta N) : \left\{ \frac{K_{\max}(k\cdot\Delta N)}{f(L_R)}\bigg|_{p=1\cdots3} \le \frac{K_{IC,char}}{\eta_{K_{IC}}} \right\}_{j=1\ldots n_{steps}} \tag{28}$$

where n_{steps} is the number of load steps considered. The map of the permissible defect then changes dramatically (Fig. 10d), because there is severe reduction of allowable defects for those regions (the interior of disc hub) where there are the highest thermal stresses at startups.[8]

CONCLUSIONS

Rotor discs for gas turbines are heavy components usually designed following a safe-life approach. However, in such a component, there is the possible occurrence of defects, and therefore, defect acceptance criteria have to be defined for the different rotor regions (considering stress distribution and temperature).

The assessment requires the adoption of probabilistic approaches because of the number of variables (stress components, material properties and sizing error of NDT) involved in the structural integrity of turbine discs. First, the research has dealt with the probabilistic assessment of rotor discs by state-of-the-art procedures under fatigue and static fracture. The analysis has shown that the capability to withstand a prospective overspeed at the end of the target lifetime is the key assessment, together with an identification of the random variables, which control the failure probability.

Then, a semi-probabilistic approach, based on *partial safety factors*, has been introduced and tuned on the basis

of probabilistic analyses in order to achieve a target failure probability of $5 \cdot 10^{-5}$ during the service life. The method has been incorporated into a new numerical framework, named AStrID, which allows the automatic calculation of the residual lifetime critical and the permissible defect for a rotor disc component in presence of surface and internal defects. The software allows us to obtain contour maps, which represent a very effective and ready-to-use tool for the determination of the most critical region of the component.

Acknowledgements

The present work has been developed in collaboration with Ansaldo Energia Spa (AEN) within a research contract, under the direction of S. Beretta, about methods for structural integrity assessment of rotor discs in presence of defects. The authors acknowledge permission of AEN to publish the paper. M. Madia worked at the research project when he was employed at Politecnico di Milano. E. Cavalleri was the project manager of the research for the industrial partner.

REFERENCES

1 Corran, R. S. J. and Williams, S. J. (2007) Lifting methods and safety criteria in aero gas turbines. *Eng. Fail. Anal.*, **14**, 518–528.
2 Muehle, E. E and Ewald, J. (1990) High-reliability steam turbine components – material and strength calculation aspects. In *High Temperature Materials for Power Engineering*. Kluwer Academic Publishers, Dordrecht.
3 Boyd-Lee, A. D., Harrison, G. F. and Henderson, M. B. (2001) Evaluation of standard life assessment procedures and life extension methodologies for fracture-critical components. *Int. J. Fatigue*, **23**, 11–19.
4 Beretta, S., Foletti, S. and Sanguineti, A. (2014) A simple format for the definition of safety factor for LCF. Paper GT2014-26457. In *Proceedings of ASME Turbo Expo 2014*, ASME.
5 Endres, W. (1992) Rotor design for large industrial gas turbines. *Paper 92-GT-273*, ASME.
6 William, E. N. and Monroe, P. C. (1997) Understanding and preventing steam turbine overspeeds. In *Proc. 26th Turbomachinery Symposium*, 129–142.
7 Clark, E. E. (1996) Rotating equipment loss prevention – an insurer's viewpoint. In *Proc. 25th Turbomachinery Symposium*, 103–122.
8 Florjancic, S. S., Pross, S. and Eschbach, U. (1997) Rotor design in industrial gas turbines. *Paper 97-GT-75*, ASME.
9 Janssen, M. J. and Joyce, J. S. (1996) 35-year old splined-disc rotor design for large gas turbines. *Paper 96-GT-523*, ASME.
10 Dillström, P. and Nilsson, F. (2003) Probabilistic fracture mechanics. In: *Comprehensive Structural Integrity*, vol. **7**: (Edited by R. A. Ainsworth and K. H. Schwalbe), Elsevier, Amsterdam, NL.
11 ISO EN 1990. (2002) *Eurocode 0: Basis of Structural Design*. ISO, Geneva, CH.
12 BS 7910. (2005) *Guide on Methods for Assessing the Acceptability of Flaws*. BSI Standards, London, UK.
13 Wu, Y. T., Enright, M. P. and Millwater, H. R. (1992) Probabilistic methods for design assessment of reliability with inspection. *AIAA J.*, **40**, 937–946.
14 API 579-1/ASME FFS-1. (2007) *Fitness-for-service*. American Petroleum Institute, Washington, US.
15 Dillström, P. (2000) ProSINTAP – a probabilistic program implementing the SINTAP assessment procedure. *Eng. Fract. Mech.*, **67**, 647–668.
16 Gollwitzer, S., Kirchgäßner, B., Fischer, R. and Rackwitz, R. (2006) PERMAS-RA/STRUREL system of programs for probabilistic reliability analysis. *Struct. Saf.*, **28**, 108–129.
17 Leverant, G. R., Millwater, H. R., McClung, R. C. and Enright, M. P. (2004) A new tool for design and certification of aircraft turbine rotors. *J. Eng. Gas Turbines Power*, **126**, 155–159.
18 McClung, R. G., Lee, Y. D., Enright, M. P. and Liang, W. (2012) New methods for automated fatigue crack growth and reliability analysis. Paper GTP-12-1174. In *Proc. ASME Turbo Expo 2012*, ASME.
19 Wormsen, A., Fjelstadt, A. and Harkegard, G. (2008) A post – processor for fatigue crack growth analysis based on a finite element stress field. *Comput. Methods Appl. Mech. Eng.*, **197**, 834–835.
20 Vormwald, M. and Seeger, T. (1991) The consequences of short crack closure on fatigue crack growth under variable amplitude loading. *Fatigue Fract. Eng. Mater. Struct.* , **14**, 205–225.
21 Radaj, D. and Vormwald, M. (2013) Elastic–plastic fatigue crack growth. In *Advanced Methods of Fatigue Assessment*, Springer, Berlin, DE, pp. 391–481.
22 McClung, R. and Sehitoglu, H. (1988) Closure behavior of small cracks under high strain fatigue histories. In: *Mechanics of Fatigue Crack Closure*(*Edited by* J. C. Newman and W. Elber), ASTM-STP 982, ASTM, Philadelphia, US.
23 Newman, J. C. Jr. (1981) A crack-closure model for predicting fatigue crack growth under aircraft spectrum loading. In: *Methods and Models for Predicting Fatigue Crack Growth under Random Loading*(*Edited by* J. B. Chang and C. M. Hudson), ASTM STP 748. ASTM, Philadelphia, US.
24 Harkegard, G., Denk, J. and Stark, K. (2005) Growth of naturally initiated fatigue cracks in ferritic gas turbine rotor steels. *Int. J. Fatigue*, **27**, 715–726.
25 Foletti, S., Beretta, S., Scaccabarozzi, F., Rabbolini, S. and Traversone, L. (2015) Fatigue crack growth in blade attachment of turbine disks: experimental tests and life prediction. *Mater. Performance Char.*, **4**, 182–197.
26 Newman, J. C. (1992). Fracture mechanics parameters for small cracks In: *Small Crack Test Methods* (*Edited by* J. M. Larsen and J. E. Allison). ASTM-STP 1149, ASTM, Philadelphia, US.
27 Rabbolini, S., Beretta, S., Foletti, S., Riva, A. (2015) Short crack propagation in LCF regime at room and high temperature in Q & T rotor steels. *Int. J. Fatigue*, **75**, 10–18.
28 Forsberg, F. (2008) Probabilistic assessment of failure risk in gas turbine discs. Master's thesis, Linkoping University, SE.
29 Zerbst, U., Schödel, M., Webster, S. and Ainsworth, R. A. (2007) *Fitness-for-service Fracture Assessment of Structures Containing Cracks – A Workbook Based on the European SINTAP/FITNET Procedure*. Elsevier, Amsterdam, NL .
30 R6-Revision 4. (2013) *Assessment of the Integrity of Structures Containing Defects*. EDF Energy Nuclear Generation Ltd., Gloucester, UK.
31 Newman, J. C. and Raju, I. S. (1981) An empirical stress intensity factor equation for the surface crack. *Eng. Fract. Mech.*, **2**, 185–192.

32 Shiratori, M., Miyoshi, T. and Tanikawa, T. (1986) Analysis of stress intensity factors for surface cracks subjected to arbitrarily distributed surface stresses. In: *Stress Intensity Factors Handbook* (Edited by Y. Murakami (1987)), Pergamon Press, Oxford, UK, pp. 725–27.
33 Madia, M., Beretta, S., Foletti, S. and Cavalleri, E. A. (2013) A tool for the structural integrity assessment of turbine disks: probabilistic and numerical background. Paper GT2013-96029. In *Proceedings of ASME Turbo Expo*, ASME.
34 Zerbst, U., Ainsworth, R. A. and Madia, M. (2012) Reference load versus limit load in engineering flaw assessment: a proposal for a hybrid analysis option. *Eng. Fract. Mech.*, **91**, 62–72.
35 Madia, M., Arafah, D. and Zerbst, U. (2014) Reference load solutions for plates with semi-elliptical surface cracks subjected to biaxial tensile loading. *Int. J. Press. Vessels Pip*, **119**, 19–28.
36 Miura, N. and Y. Takahashi (2010) Evaluation of *J*-integral for surface cracked plates under biaxial loading using extended reference stress method. *Int. J. Press. Vessels Pip*, **87**, 58–65.
37 L. Scolavino, M. Madia, Beretta, S. and Zerbst, U. (2014) Critical speed of flawed rotors: global vs. local approach. Paper GT2014-26881. In *Proceedings of ASME Turbo Expo*, ASME.
38 Annis, C. (2004) Probabilistic life prediction isn't as easy as it looks. In: *Probabilistic Aspects of Life Prediction* (*Edited by* W. S. Johnson and B. M. Hilberry), *ASTM STP 1450*. ASTM, Philadelphia, US.
39 FAA. (1993) *Damage Tolerance Assessment Handbook*, Federal Aviation Administration, Volpe National Transportation Systems Center, Cambridge, US.
40 Wallin, K. (2002) Master curve analysis of the 'Euro' fracture toughness dataset. *Eng. Fract. Mech.*, **69**, 451–481.
41 Krautkramer, J. and Krautkramer, H. (1990) *Ultrasonic Testing of Materials*. Springer, Berlin, DE.
42 Kassir, M. K. and Sih, G. C. (1966) Three-dimensional stress distribution around an elliptical crack under arbitrary loading. *J. Appl. Mech.*, **33**, 601–611.
43 Murakami, Y. and Nemat-Nasser, S. (1983) Stability of interacting surface flaws of arbitrary shape. *Eng. Fract. Mech.*, **17**, 193–210.
44 Murakami, Y. and Isida, M. (1985) Analysis of arbitrarily shaped surface crack and stress field at crack front near surface. *Trans. Jap. Soc. Mech. Engrs. Ser. A*, **51**, 1050–1056.
45 Carboni, M. (2012) A critical analysis of ultrasonic echoes coming from natural and artificial flaws and its implications in the derivation of probability of detection curves. *Insight*, **54**, 208–216.
46 Dai, D. N., Hills, D. A., Harkegard, G. and Pross, J. (1998) Simulation of the growth of near surface defects. *Eng. Fract. Mech.*, **59**, 415–424.
47 Isida, M. and Noguchi, H. (1987) Tension of a plate containing an embedded elliptical crack. In: *Stress Intensity Factors Handbook* (*Edited by* Murakami Y.), Pergamon Press, Oxford, pp. 734–741.
48 Sedlacek, G. and Kraus, O. (2007) Use of safety factors for the design of steel structures according to Eurocodes. *Eng. Fail. Anal.*, **14**, 434–441.